Journal of Drug Delivery Science and Technology 125 (2026) 108671

Contents lists available at ScienceDirect

Journal of Drug Delivery Science and Technology

journal homepage: www.elsevier.com/locate/jddst

Comparing the impact of various sucrose concentrations on the performance of various lipid-based nanoformulations for the delivery of trans-resveratrol as a model drug

Anila Mathew Thevarkattil [a], Kajanthan Balasundaram [a], Nozad Hussein [b], Huner Omer [b], Sakib Yousaf [c], Chahinez Houacine [d], Adeeb Shehzad [e], Ruba Bnyan [f], Abdelbary Elhissi [g], Iftikhar Khan [a,*]

[a] School of Pharmacy and Biomolecular Sciences, Liverpool John Moores University, Liverpool, L3 3AF, United Kingdom
[b] College of Pharmacy, Hawler Medical University, Erbil, Iraq
[c] School of Pharmacy, Optometry and Medical Sciences, University of Bradford, BD7 1DP, United Kingdom
[d] School of Pharmacy and Biomedical Sciences, University of Central Lancashire, Preston, PR1 2HE, United Kingdom
[e] Biodiversity Unit, Research Center, Dhofar University, Salalah, 211, Oman
[f] School of Life Sciences, Pharmacy and Chemistry, Kingston University, London, KT1 2EE, United Kingdom
[g] Department of Pharmaceutical Sciences, College of Pharmacy, QU Health, Qatar University, Doha, Qatar

ARTICLE INFO

Keywords:
Sucrose
Nebulization
Pulmonary system
Non-invasive
Nanoformulations
Lipid-based formulations
Viscosity

ABSTRACT

Drug delivery *via* aerosolization is a non-invasive and ideal method for targeting the pulmonary system, achieving localized effect. This study aims to formulate and compare five different types of lipid-based powder formulations: pro-micelles (F1-F3), pro-niosomes (F4-F6), pro-liposomes (F7-F9), pro-transfersomes (F10-F12), and pro-nanostructured lipid carriers (F13-F15), using three different lipid-to-sucrose carrier ratios (1:05, 1:10, and 1:15 w/w) *via* a slurry method, using a model anticancer drug, trans-resveratrol (TRES). Aerosolization performance was determined *via* a two-stage impinger (TSI) paired with two medical nebulizers (i.e., air-jet and vibrating mesh). Post-hydration, vesicles from pro-niosome formulations (F3-F6) demonstrated significantly larger particle size (>1200 nm), while from pro-transfersomes (F11-F13) showed smaller particle size (<125 nm). Entrapment efficiency for all formulations exceeded 90%. An elevated dynamic viscosity was recorded for all formulations when employing a type B Ostwald viscometer as opposed to A, C and D, regardless of formulation type. Upon nebulization, the vibrating mesh nebulizer was associated with an extended nebulization time (23-32 min), short sputtering time (1.57-5.59) and high mass output (79-95%) in compared to air-jet nebulizer (irrespective of formulation type). Both nebulization time and mass output increased significantly with increasing sucrose concentration in formulations (from 1:5 to 1:15 w/w ratio). Upon aerosolization performance, the vibrating mesh showed a significantly higher emitted dose (ED; 72-98%) and fine particle fraction (FPF; 60-81%) than its counterpart nebulizer. The *in-vitro* release profile depicted zero-order controlled drug release. Moreover, over a period of 24 h, the maximum release of TRES was found at pH 5, rather than at pH 7. Thus, it was concluded that formulations with a higher viscosity (with increasing sucrose concentration) and a vibrating mesh nebulizer are the best combination for peripheral drug deposition.

1. Introduction

Globally, lung cancer is the second most prevalent malignant cancer with the highest fatality rate of all malignancies [1]. It is broadly categorized histologically into either small cell lung cancer (SCLC) and non-small cell lung cancer (NSCLC) (with NSCLC accounting for more than 85% of lung cancer patients globally) [2]. Despite commonly being a first-line treatment, systemic chemotherapy often affects non-cancerous cells, leading to significant side effects and limited effectiveness. In contrast, administering anticancer drugs through inhalation allows high concentrations of chemotherapeutic agents to be delivered directly to the lungs, providing a localized effect that enhances

* Corresponding author.
E-mail addresses: I.Khan@ljmu.ac.uk, iftikharkhans@yahoo.com (I. Khan).

https://doi.org/10.1016/j.jddst.2026.108671
Received 9 February 2026; Received in revised form 22 May 2026; Accepted 2 July 2026
Available online 2 July 2026

Table 1
Pro-micelles (F1-F3), pro-niosomes (F4-F6), pro-liposomes (F7-F9), pro-transfersomes (F10-F12), and pro-nanostructured lipid carriers (pro-NLCs) (F13-F15) were prepared using three different lipid phase-to-sucrose ratios (1:05, 1:10, and 1:15 w/w). Lipid phase (1000 mg) was prepared by using different components corresponding to a different type of formulation including; pro-micelle (Tween 80), pro-niosome (Tween 80 and cholesterol; 2:1 w/w ratio), pro-liposome (SPC), pro-transfersome (Tween 80 and SPC; 1:2 w/w ratio), and pro-NLCs (Tween 80, Compritol 888, and Miglyol 840; 1:2:2 w/w/w ratio). TRES (50 mg) was used as a model drug in all formulations.

Formulations	Lipid phase					Carrier	Ratios
	Tween-80 (mg)	SPC (mg)	Cholesterol (mg)	Compritol 888 (mg)	Miglyol 840 (mg)	Sucrose (mg)	Lipid phase-to-carrier (w/w)
Pro-micelle							
F1	1000	-	-	-	-	5000	1:05
F2	1000	-	-	-	-	10000	1:10
F3	1000	-	-	-	-	15000	1:15
Pro-niosome							
F4	666.67	-	333.33	-	-	5000	1:05
F5	666.67	-	333.33	-	-	10000	1:10
F6	666.67	-	333.33	-	-	15000	1:15
Pro-liposome							
F7	-	1000	-	-	-	5000	1:05
F8	-	1000	-	-	-	10000	1:10
F9	-	1000	-	-	-	15000	1:15
Pro-transfersome							
F10	333.33	666.67	-	-	-	5000	1:05
F11	333.33	666.67	-	-	-	10000	1:10
F12	333.33	666.67	-	-	-	15000	1:15
Pro-NLC							
F13	200	-	-	400	400	5000	1:05
F14	200	-	-	400	400	10000	1:10
F15	200	-	-	400	400	15000	1:15

antitumor activity whilst minimizing systemic side effects [3]. Nanoparticles have shown superior performance over traditional dosage forms by improving efficacy, reducing side effects, and increasing stability, thanks to their small size, larger surface area, and precise targeting capabilities [4,5].

Resveratrol (3,5,4-trihydroxystilbene), a natural polyphenol stilbene comprising two phenol rings joined together by ethylene bridges, existing in two isomeric forms, *cis*- and *trans*-resveratrol. Antioxidant, anti-inflammatory, cardioprotective, and cancer-fighting actions are some of the benefits associated with the phytoestrogen trans-resveratrol (TRES). The *trans*-form is more biologically active, but less stable, as it converts to the *cis*-form when exposed to UV light and at higher pH levels [6]. Additionally, TRES undergoes extensive liver metabolism and has poor water solubility, leading to low bioavailability [7,8]. This compound has acquired considerable attention related to its chemopreventive and anticancer properties. Comprehensive *in-vitro* and *in-vivo* research has shown that TRES can disrupt all phases of carcinogenesis, encompassing tumour initiation, development, and advancement, while also inhibiting angiogenesis and metastasis [9]. It exerts its effects by altering many signalling pathways associated with cell proliferation, inflammation, apoptosis, and tumour formation, including the Akt, NF-κB, and MAPK pathways [9]. Furthermore, recent studies have demonstrated its capacity to induce apoptosis, inhibit metastasis, and modulate the tumour microenvironment across multiple cancer types [10]. Although TRES is not a traditional chemotherapeutic agent, the recognised anticancer properties of TRES endorse its application as a model bioactive chemical in cancer research.

Previous studies have shown that transfersomes and liposomes face stability concerns due to issues such as aggregation, fusion, and leaking of drugs from the vesicles, attributed to the phospholipid component [11]. Similar instability has been observed in aqueous suspensions of niosomes and micelles [12]. To address these problems, lipid-based nanoformulations have been developed in powder form using carbohydrate carriers such as sucrose and lactose [13–15]. These carriers act as dispersing agents and emulsifiers, aiding in the breakdown of lipid-based vesicles into smaller, more stable particles by preventing phase separation and sedimentation. Additionally, carbohydrate carriers enhance viscosity and modify the rheological properties of lipid-based formulations. Therefore, pro-lipid-based dry powders are superior to lipid-based suspensions due to their enhanced stability, higher drug loading capacity, controlled and sustained drug release, reduced risk of aggregation, longer shelf life, and ease of reconstitution [16].

Aerosol production suitable for pulmonary delivery is heavily influenced by the interplay between the working mechanism of various nebulizers and the physicochemical parameters of the formulations, such as pH, viscosity, and surface tension [6,17]. In the case of pulmonary disease conditions, nebulized vesicles improve the residence time of drugs in the lungs, potentially improving therapeutic impact, without causing substantial systemic adverse effects [18]. To study the particle deposition, the British Pharmacopeia recommends using an artificial lung model called the two-stage or twin impinger (TSI). The TSI, with upper and lower stages and a cut-off diameter of 6.4 μm between them, simulates the upper and lower respiratory tracts to measure drug deposition in the lungs. Formulation deposition in the lungs occurs through three main mechanisms: inertial impaction, sedimentation, and diffusion, all of which depend on the particle aerodynamic diameter [19].

In this study, several lipid-based formulations (pro-micelles, pro-niosomes, pro-liposomes, pro-transfersomes, and pro-nanostructured lipid carriers (pro-NLCs)) were investigated in order to assess their viability as reconstituted dry powder nanoformulations for pulmonary administration through nebulization. These various formulations correspond to different classes with distinct structural characteristics, including surfactant micelles, non-ionic surfactant vesicles, phospholipid vesicles, and lipid matrix nanoparticles [20–27]. Due to these structural differences, the formulations behave differently during dehydration (i.e., in a rotary evaporator), storage, and rehydration. Therefore, investigating multiple lipid-based pro-powder systems facilitates a systematic evaluation of their ability to form stable dry formulations and reconstituted nanoscale dispersions upon hydration suitable for nebulization [28–30], making them suitable for nebulization. Moreover, excipients for the dry-lipid-based powder formulations were chosen based on their proven and defined functional roles in creating distinct nanocarrier systems. Pro-micelles (F1–F3) were formulated utilizing amphiphilic surfactants (e.g., Tween 80) in order to facilitate micelle formation. Pro-niosomes (F4–F6) consisted of non-ionic surfactants including Tween 80 or Span 60 with cholesterol for bilayer formation. Pro-liposomes (F7–F9) employed phospholipids (e.g., soy or egg

lecithin) with or without cholesterol to create stable vesicles. Pro-transfersomes (F10–F12) included phospholipids with edge activators (Span 80 or Tween 80) to enhance membrane flexibility. Pro-nanostructured lipid carriers (F13–F15) were prepared using a mixture of liquid and solid lipids along with an edge activator to enhance drug accommodation. Sucrose, as a carbohydrate sugar, was employed as a hydrophilic carrier due to its high solubility as well as suitability for producing free-flowing powders [31,32]. Various lipid-to-sucrose ratios (1:5, 1:10, and 1:15 w/w) were explored to assess their effect on formulation properties as well as aerosol generation and deposition in the pulmonary system. In this study, formulations were characterized based on particle size, drug entrapment, viscosity, and *in-vitro* drug release. The performance of nebulizers was assessed *via* deposition of a drug in the TSI. The aim was to explore how the viscosity of each formulation influenced nebulization performance, specifically nebulization time, sputtering time, and mass output, using two types of nebulizers: air-jet and vibrating mesh. Finally, the deposition of TRES in the nebulizer reservoir and the stages of the TSI were analyzed to determine the most effective nebulizer and formulation type.

2. Materials and methods

2.1. Materials

Soya phosphatidylcholine (SPC; Lipoid S-100) was purchased from Lipoid, Switzerland. Trans-resveratrol (TRES) was obtained from Manchester Organics Ltd., UK. Propylene glycol dicaprylate (PGD; Miglyol 840) was generously gifted by IOI Oleochemicals, Witten, UK. Glycerol dibehenate (GDB; Compritol 888 ATO) was a gift from Gattefosse, France. Tween 80 and cholesterol were acquired from Sigma Aldrich, UK. HPLC grade acetonitrile, analytical grade sucrose, formic acid, acetic acid, absolute ethanol, and tetrahydrofuran were bought from Fischer Scientific, UK. Spectra/Por 7 pre-treated dialysis membrane (MWCO: 3.5 kDa) was procured from Spectrum Laboratories, USA.

2.2. Preparation of pro-micelles formulations via slurry method

A slurry method was adopted to prepare pro-micelle formulations [33]. Three different formulations (F1, F2 and F3) were prepared using a single concentration of surfactant (Tween 80; 1000 mg) as a lipid phase, and three different concentrations of sucrose (5000, 10000 and 15000 mg) as a carbohydrate carrier. TRES (50 mg) was employed as the model drug (Table 1). In each pro-micelle formulation, Tween 80 and TRES were dissolved in ethanol (20 mL) and poured over sucrose carrier in a 100 mL round bottom flask (RBF) to make a slurry. The RBF was then attached to a rotary evaporator (Buchi Rotavapor R-114, Switzerland). A rotary equipped with a water bath (Buchi Water Bath B-480, Switzerland) was previously adjusted at 45 °C, where the round bottom flask (RBF) was immersed in a hot water bath at a rotation speed of 270 rpm. This helped ethanol evaporate as droplets, and the negative pressure created by a vacuum pump (Buchi Vac V-501) then transported these droplets to the condenser, where upon condensation the organic solvent was collected in a receiving flask. Upon complete evaporation, the negative pressure was released, the RBF was detached, and the dry powder pro-micelle formulation was collected and stored at −18 °C for subsequent studies.

2.3. Preparation of pro-niosome formulations

Pro-niosomes were manufactured through the slurry method detailed in Section 2.2, utilizing a rotary evaporator. Amongst the pro-niosome formulations, three formulations (F4, F5, and F6) were created, combining surfactant (Tween 80) and cholesterol as the lipid phase (1000 mg) in a 2:1 w/w ratio. Additionally, sucrose was incorporated in three different concentrations (5000, 10000 and 15000 mg) at 1:05, 1:10 and 1:15 w/w lipid phase-to-carrier ratio (Table 1).

2.4. Preparation of pro-liposome formulations

The slurry method, along with a rotary evaporator, was employed to create pro-liposomal formulations (F7, F8, and F9) following the procedure detailed in Section 2.2. These formulations consisted of phospholipid (SPC) (1000 mg) as the lipid phase, along with a drug TRES (50 mg), and three varying concentrations of sucrose (5000, 10000 and 15000 mg) to establish different lipid-to-carrier ratios (1:05, 1:10 and 1:15 w/w), as indicated in (Table 1).

2.5. Preparation of pro-transfersome formulations

Pro-transfersome formulations (F10, F11, and F12) were prepared using the slurry method (Section 2.2). The lipid phase consists of Tween 80 and SPC (1000 mg) in a 1:2 w/w ratio (333.33:666.67 mg), along with a consistent amount of TRES (50 mg). Sucrose was selected as a carbohydrate carrier in three different concentrations to manufacture formulations in 1:05, 1:10 and 1:15 w/w lipid phase-to-carrier ratio (Table 1).

2.6. Preparation of Pro-NLC formulations

Pro-NLCs (F13, F14 and F15) were manufactured using the slurry method (Section 2.2). In preparation of these formulations *via* rotary evaporator, surfactant (Tween 80), solid lipid (Compritol 888), and liquid lipid (Miglyol 840) were incorporated as a lipid phase (1000 mg) in a 1:2:2 w/w/w ratio, and TRES as a drug (50 mg), whereas a carbohydrate carrier (sucrose) was employed in three different concentrations (5000, 10000 and 15000 mg) as lipid phase-to carrier-ratios (i.e., 1:05, 1:10 and 1:15 w/w) (Table 1).

2.7. Drug-excipient interaction study using Fourier Transform-Infrared Spectroscopy (FTIR)

FTIR spectra were recorded using the Cary 630-FTIR (Agilent Technologies, USA) equipped with a single reflection pure diamond attenuated total reflectance (ATR) crystal sample interface. A sample of 10–15 mg of the starting materials (i.e., TRES, Tween 80, SPC, cholesterol, Miglyol 840, and Compritol 888) and all formulations (F1–F15) were measured by contacting them directly with the ATR crystal (the hammer above the crystal was only used for solid samples) in the spectral range of 4000–650 cm^{-1}. Each sample underwent three separate measurements (each time a fresh aliquot was used). Each spectrum was generated from four scans with a resolution of 4 cm^{-1}.

2.8. Powder X-ray diffraction (PXRD) analysis

TRES, coarse sucrose carrier, and all prepared powder formulations (F1–F15) were studied *via* PXRD (Rigaku Miniflex, Rigaku Ltd., Tokyo, Japan) using a diffracted beam monochromator with Cu-Kα ($\lambda = 0.154$ nm). Each sample was loaded onto a silicon standard sample holder, and the intensity of diffraction was recorded at an angle of 2θ between the angular range of 5-55° using a scanning rate of 2°/min. The experiment was carried out using a 30 kV voltage and 15 mA current. The scan peaks from individual ingredients and formulations were examined and compared with respect to their crystalline form.

2.9. Morphology study

The surface morphology of the coarse sucrose carrier, TRES, and pro-lipid-based powder formulations (F1–F15) was analyzed using SEM (EFI Quanta 200, Brno, Czech Republic). Each sample was placed onto aluminium stubs (previously coated with a carbon-coated film), and the deposited excess powder was removed with an air spray. Prior to loading for imaging, each sample stub was coated with a thin platinum layer using a sputter coater (Emitech K550x Sputter Coater, Kent, UK) for

2 min under vacuum. Samples were examined, and images were captured under various magnifications at 20 kV.

2.10. Hydration and annealing of lipid-based powder formulations

Each formulation type (pro-micelle, F1–F3; pro-niosome, F4–F6; pro-liposome, F7–F9; pro-transfersome, F10–F12; and pro-NLC, F13–F16) was prepared in three different lipid phase-to-carrier ratios (i.e., 1:05, 1:10 and 1:15 w/w). For hydration, each pro-lipid-based powder formulation (F1–F15) was hydrated in 80 mL of deionized water (DW), which corresponds to 75, 137.50 and 200 mg of pro-lipid-based formulation per 1 mL of DW, respectively. After the addition of DW, each sample was vortexed (Fisons WhirliMixer, Fisons Scientific Equipment, UK) for 5 min to ensure complete dissolution of sucrose carrier particles and dispersion/hydration of the lipid phase. The formulations were then left to anneal at room temperature for 2 h to stabilize lipid particles.

2.11. Nano sizing via probe sonication

Particle sizes of lipid-based formulations (F1–F15) were reduced to the nanometer range using probe sonication (Qsonica Probe Sonicator, Newtown, CT, USA) for a total duration of 9 min (2 min treatment and 1 min rest time for 3 cycles) at an amplitude intensity of 80%. The extended duration of sonication time and high amplitude intensity may cause leaching/generation of titanium particles (associated with mechanical erosion of the sonication probe tip, typically made of titanium or titanium alloy). To remove these titanium particles as contaminants from the nanoformulations, bench centrifugation (Hermle Labortechnik GmbH, Germany) was conducted at 1000 rpm (i.e., 1250 g) for 8 min. This lower centrifugal force facilitated sedimentation of the titanium particles to the bottom of the centrifuge tube, following which the supernatant was removed as uncontaminated by titanium particles for further studies.

2.12. Particle size, polydispersity index and zeta potential analysis

Prior to analysis, each formulation was subjected to a 1:9 v/v dilution using DW. Particle size and polydispersity index (PDI) of all formulations (F1–F15) were measured using dynamic light scattering (DLS) *via* Zetasizer Nanoseries (Malvern Zetasizer Nano series, Malvern, Worcestershire, UK). Zeta potential was determined employing Laser Doppler Velocimetry (LDV) *via* electrophoretic mobility in the dispersion medium, where an electric field was applied to dispersed particles, which then moved with a velocity related to their zeta potential.

2.13. Entrapment efficiency of TRES in formulations via HPLC

The entrapment efficiency of TRES-loaded lipid-based formulations was determined by identifying the amount of unentrapped and total drug. The unentrapped drug was quantified by pipetting 0.5 mL of formulation into a Millipore filter (3 kDa; Fisher Scientific, Loughborough, UK), and bench centrifugation (Spectrafuge 24D, Labnet International, Edison, NJ, USA) was conducted for 15 min at 8000 rpm (5900 g). The unentrapped or free TRES was allowed to pass through the Millipore filter and sedimented as a filtrate at the bottom of the tube, which was then analyzed *via* HPLC (Agilent 1200 Series Instrument, Waldborn, Germany), while the entrapped TRES in the vesicles/particles was retained by the filter. For total drug analysis *via* HPLC, 0.5 ml of each formulation was diluted with 4.5 ml of a mobile phase (acetonitrile and 0.1% formic acid in DW (1:1 v/v)). The entrapment efficiency of TRES in formulations was calculated using Eq. (1)

$$\text{Entrapment efficiency}\ (\%) = \left(\frac{\text{Total drug} - \text{Unentrapped drug}}{\text{Total drug}}\right) \times 100 \quad \text{(Eq. 1)}$$

TRES quantification was achieved through HPLC using a gradient elution method, where two solvents were employed as a mobile phase for a total run time of 15 min. The mobile phase elution profile consisted of 10:90% acetonitrile and DW (0.1% formic acid) for 0 min; 85:15% acetonitrile and DW (0.1% formic acid) for 13 min; and 90:10% acetonitrile and DW (0.1% formic acid) for 15 min. The flow rate of mobile phase was set at 1 mL/min, using a wavelength of 306 nm. A Luna C-18, 5 μm, 250 mm × 4.6 mm (Phenomenex, Torrance, CA, USA) column was used as a stationary phase. An injection volume of 20 μl was employed with a column temperature of 25 °C. A calibration curve of TRES (1–100 μg/mL) was constructed for the quantification of unknown TRES concentrations [6].

2.14. Measurement of fluid viscosity of lipid-based formulations

To study the influence of the viscosity of lipid-based formulations on nebulization time, nebulization performance, and *in-vitro* drug release, two different types of equipment were used to measure viscosities. The Ubbelohde viscometers (U-tube) (VWR, Leicestershire, UK) and a hybrid rheometer (TA HR10, Discovery Series, USA) were used to measure the dynamic viscosity, in which the way a liquid flows in response to applied external force (tangential force) per unit surface, known as shearing stress, was measured and expressed in pascals.

2.14.1. Ubbelohde viscometers

To determine the viscosity of all formulations (F1–F15), four different types of U-tube viscometers (A, B, C and D) were used based on their internal diameter at a temperature of 20 ± 0.1 °C. The time required for the level of the lipid-based formulations to drop from one mark to the next was measured using a stopwatch in seconds. Kinematic viscosity was measured using Eq. (2), where t is the time taken for the liquid to flow, and k is the viscometer constant which is determined by measuring the time taken for a DW of known viscosity to flow. The k values for viscometer A, B, C and D were 0.003, 0.010, 0.030 and 0.100, respectively.

$$V\left(m^2/\sec\right) = kt \quad \text{(Eq. 2)}$$

The dynamic viscosity (η) of each formulation was expressed from Eq. (3), where ρ is the density of each formulation. It measures the resistance to flow when an external force is applied.

$$\eta = k\rho t \quad \text{(Eq. 3)}$$

2.14.2. Hybrid rheometer

The dynamic viscosity of all the formulations (F1–F15) was determined by utilizing a hybrid rheometer. Initially, the required amount of sample was trimmed, and the measurement gap was set to zero at a temperature of 25 °C. The experiment involved using a 40 mm stainless steel parallel plate for rheological measurements with the flow ramp method. Samples were tested with a 1000 μm gap, a 45,000 μm loading gap, and a 50 μm trim gap. The shear rate ranged from 1.0 to 100.0 Hz over 60 s, with a sampling interval of 1 s, following a 180-s soak time.

2.15. In- vitro aerosolization performance

For *in-vitro* aerosolization studies, an artificial lung model known as a two-stage impinger (TSI) was used along with the vibrating mesh (Omron Micro-air U22 pocket nebulizer, UK) and air jet nebulizers (PARI Turboboy 5 air jet, UK) to evaluate nebulization performance. TSI has been validated as a standard model for the examination of nebulized aerosols by the British Pharmacopeia (BP), the United States Pharmacopeia (USP), and the European Pharmacopeia (EP); hence, it was added as a performance metric.

For aerosol collection in the TSI, 7 mL of DW was added in the upper stage and 30 mL in the lower stage. After assembling the TSI stages, the airflow rate was adjusted to 15 L/min using an airflow meter (Copley

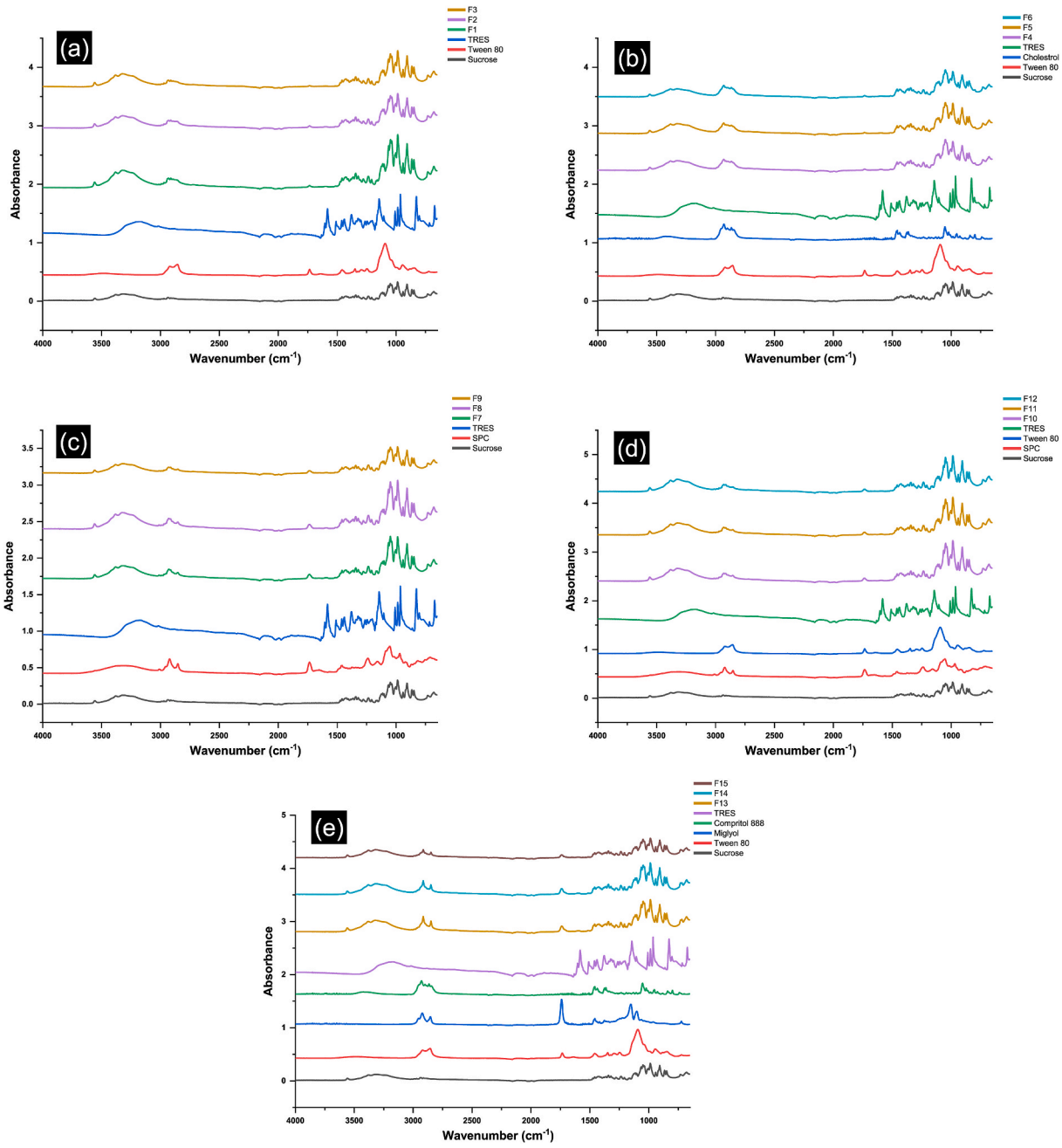

Fig. 1. The FTIR spectra for (a) pro-micelles (F1-F3), (b) pro-niosomes (F4-F6), (c) pro-liposomes (F7-F9), (d) pro-transfersomes (F10-F12), and (e) pro-NLCs (F13-F15), as well as sucrose carrier and TRES alone, were generated using varying lipid-to-sucrose carrier ratios (1:05, 1:10, and 1:15 w/w). These images are representative of three such different experiments.

Scientific, Nottingham, UK). Prior to nebulization, an aliquot of a 3 mL formulation was added to the nebulizer reservoir and placed in front of the TSI mouthpiece. Nebulization performance was conducted until dryness (i.e., no further generation of aerosol droplets). Nebulization performance was evaluated based on nebulization time, sputtering time, and mass output. The nebulization time was described as the time required for continuous aerosol generation until it became unstable or sporadic. Further tapping of the nebulizer resulted in the formation of erratic aerosolization; this period remained until dryness and was described as 'sputtering time'. Furthermore, the total or complete nebulization time was defined as the sum of the nebulization and sputtering times. The mass output was determined by measuring the difference in mass of the formulation in the nebulizer before and after nebulization using Eq. (4).

$$\text{Mass output } (\%) = \left(\frac{\text{Weight of nebulized formulation}}{\text{Weight of formulation present in the nebulizer prior to nebulization}} \right) 100 \quad \text{(Eq. 4)}$$

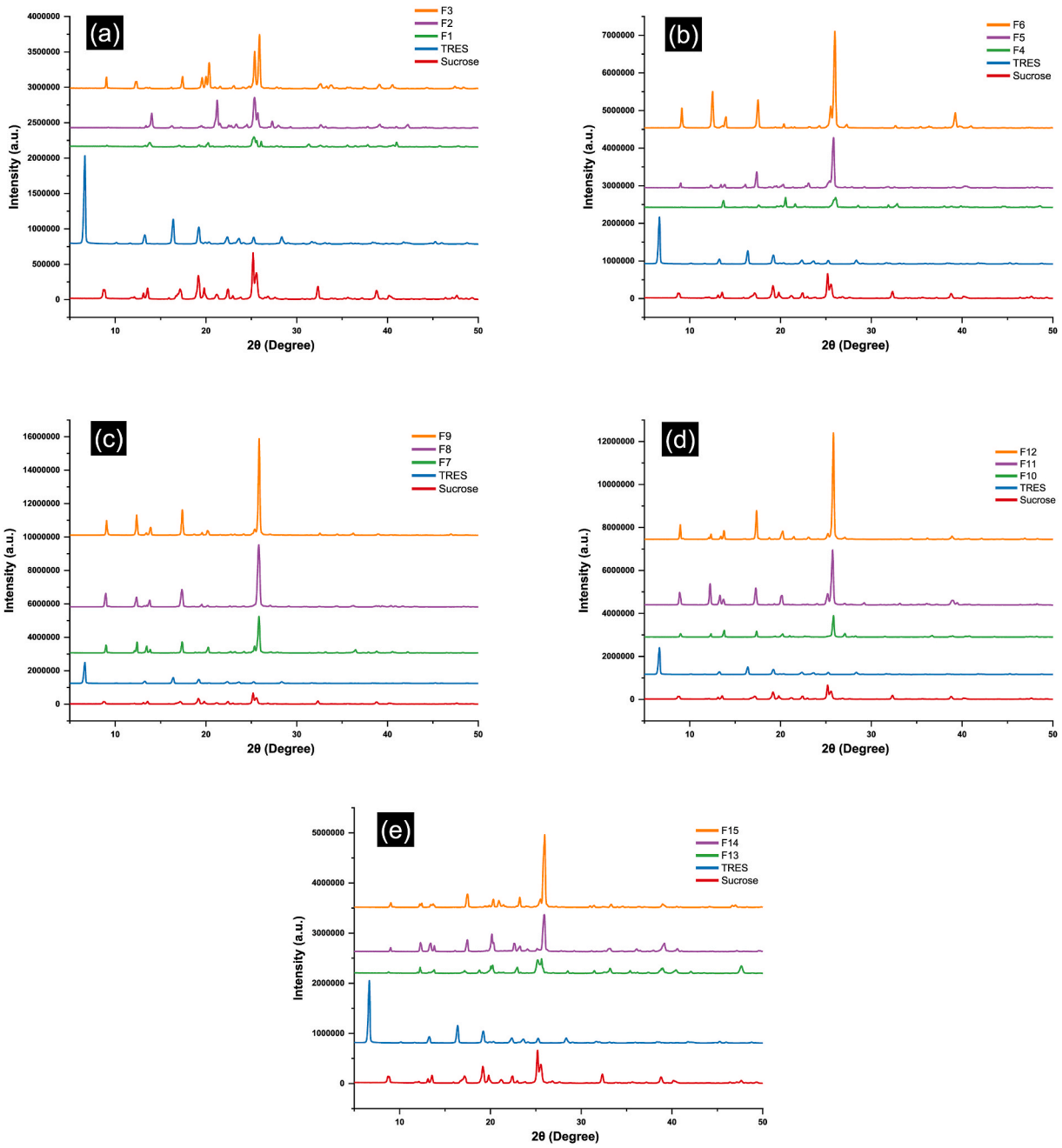

Fig. 2. PXRD spectra of sucrose and TRES alone, followed by their incorporation: (a) pro-micelles (F1-F3), (b) pro-niosomes (F4-F6), (c) pro-liposomes (F7-F9), (d) pro-transfersomes (F10-F12), and (e) pro-NLCs (F13-F15) were prepared using increasing lipid-to-sucrose carrier ratios (1:05, 1:10, and 1:15 w/w). These data are typical of three such different experiments.

Furthermore, the deposition of TRES in the two stages of TSI, as well as the remaining TRES as dead or residual volume in the nebulizer reservoir, was determined *via* HPLC post-nebulization. The amount of TRES deposited in the upper and lower stages was determined as the emitted dose (ED) (Eq. (5)). The final particle fraction (FPF) was calculated as the percentage of drug deposited in the lower stage of TSI,

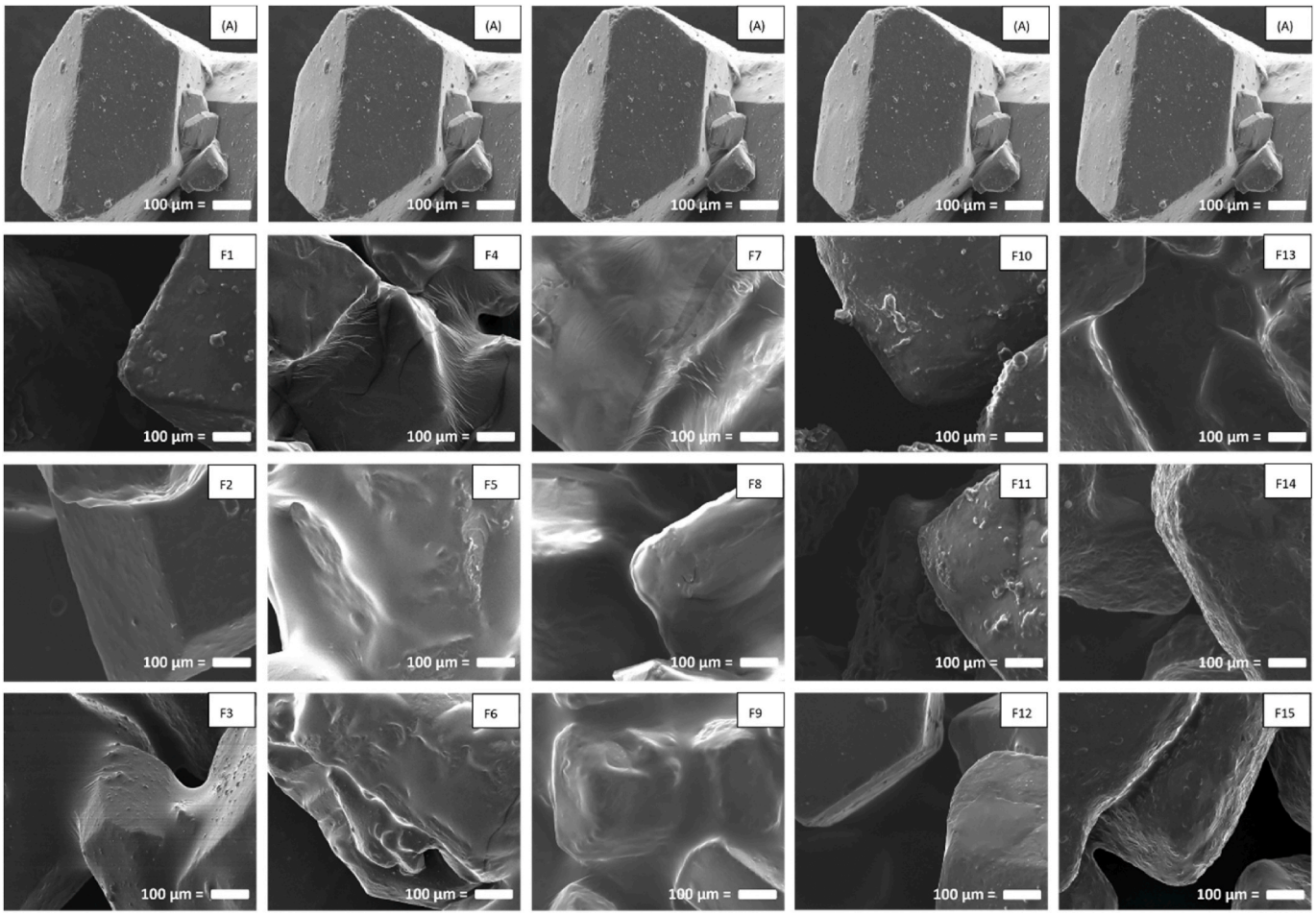

Fig. 3. SEM images of coarse sucrose (A) prior to loading with lipid phase, then formulatoins of pro-micelles (F1-F3), pro-niosomes (F4-F6), pro-liposomes (F7-F9), pro-transfersomes (F10-F12), and pro-NLCs (F13-F15) prepared using three different ratios of lipid-to-sucrose carrier (1:05, 1:10, and 1:15 w/w). These images are typical of three such different experiments.

as depicted in Eq. (6).

$$\mathrm{ED}(\%) = \left(\frac{\text{Amount of the TRES in the upper and lower stage}}{\text{Amount of the TRES in the upper and lower stage, and reservior}}\right)100 \quad \text{(Eq. 5)}$$

$$\mathrm{FPF}(\%) = \left(\frac{\text{AmountoftheTRES in the lower stage}}{\text{Amount of the TRES in the upper and lower stage, and reservior}}\right)100 \quad \text{(Eq. 6)}$$

2.16. *In-vitro release of TRES from formulations*

The *in-vitro* release study of TRES from the lipid-based nano-formulations was conducted under conditions designed to mimic the in-situ physiological environment as closely as possible. Specifically, the release medium was maintained at 37 ± 0.5 °C to simulate body temperature, and the pH was adjusted to pH 5 or pH 7. The *in-vitro* release profile of TRES from all prepared lipid-based formulations (F1–F15) was evaluated using a dialysis bag diffusion method (molecular weight cut-off: 3500 Da) in a USP dissolution apparatus (Varian Instrument, Cary, NC, USA) [34]. TRES drug release rates were tested in acetate buffer (pH 5) and DW (pH 7). The dialysis bags were filled with the formulation and immersed in 900 mL of release medium consisting of either acetate buffer (pH 5) or deionized water (DW) (pH 7). The dissolution medium

Table 2
Coarse sucrose carrier was employed to prepare pro-micelles (F1-F3), pro-niosomes (F4-F6), pro-liposomes (F7-F9), pro-transfersomes (F10-F12), and pro-NLCs (F13-F15) powder formulations, followed by their characterization using their particle size, PDI, zeta potential, and entrapment efficiency. Data are mean ± SD, n = 3.

Formulations	Particle size (nm)	PDI	Zeta potential (mV)	Entrapment efficiency (%)
F1	241.31 ± 9.10	0.21 ± 0.03	−25.30 ± 0.45	91.58 ± 4.50
F2	325.83 ± 7. 40	0.23 ± 0.02	−20.81 ± 0.30	93.02 ± 6.99
F3	405.27 ± 4.90	0.26 ± 0.01	−26.94 ± 1.10	93.29 ± 3.29
F4	1292.48 ± 8.53	0.12 ± 0.03	−33.10 ± 1.45	92.04 ± 2.74
F5	2263.51 ± 6.12	0.15 ± 0.02	−33.31 ± 1.33	92.53 ± 3.89
F6	2492.37 ± 9.24	0.16 ± 0.03	−35.60 ± 1.16	94.11 ± 5.69
F7	219.15 ± 8.63	0.24 ± 0.01	−21.70 ± 0.10	95.71 ± 3.16
F8	254.49 ± 5.16	0.25 ± 0.02	−26.59 ± 0.19	96.68 ± 2.41
F9	273.21 ± 3.38	0.25 ± 0.01	−24.09 ± 0.05	97.16 ± 3.39
F10	101.76 ± 2.08	0.35 ± 0.02	−19.72 ± 0.58	95.22 ± 3.92
F11	111.27 ± 3.60	0.37 ± 0.03	−14.51 ± 0.55	97.23 ± 3.23
F12	125.73 ± 1.30	0.37 ± 0.02	−14.16 ± 0.20	98.54 ± 2.03
F13	287.44 ± 9.03	0.22 ± 0.01	−26.91 ± 0.90	92.27 ± 2.41
F14	324.58 ± 2.61	0.21 ± 0.02	−21.50 ± 0.65	92.74 ± 2.37
F15	385.72 ± 8.33	0.28 ± 0.04	−27.40 ± 0.20	94.61 ± 4.60

was maintained under constant stirring at 100 rpm. To enhance the solubility of TRES and ensure sink conditions, 20% (v/v) methanol was incorporated into the release medium. The release study was conducted for 24 h. For each formulation (F1-F15), a 5 mL sample containing 1 mg/mL of TRES was placed in a dialysis bag and submerged in 900 mL of dissolution media. Samples of 1 mL were taken at the time intervals of 0 min, 30 min and 1, 2, 3, 4, 5, 6, 7 and 24 h, and replaced with 1 mL of fresh media to maintain sink conditions (constant volume). For the TRES release study, each sample withdrawn was analyzed *via* HPLC. The release study of TRES alone at 1 mg/mL was used as a control to compare the results and establish its release profile.

2.17. Statistical analysis

SPSS software (IBM SPSS Statistics 28.0) was used to perform one-way ANOVA and Student's t-tests on the acquired data to determine whether there was a statistically significant difference between more than two groups or two sets of data. All trials were conducted in triplicate, and a p-value less than 0.05 was considered statistically significant.

3. Results and discussion

3.1. FTIR spectroscopy for drug excipient interaction

FTIR spectroscopy was employed to examine the potential interactions among the different components of TRES lipid-based formulations, as these interactions are vital and may influence the stability and efficacy of the formulations. The FTIR spectra of all formulations (F1-F15) along with sucrose carrier and TRES are shown in Fig. 1. The FTIR spectrum of the TRES revealed intense absorption bands at 1608 cm^{-1} (aromatic C-C double-bond stretching), 1592 cm^{-1} (olefinic C-C olefinic stretching), and 966 cm^{-1} (typical trans olefinic band), indicating resveratrol presence [35]. In lipid-based powder formulations, these key peaks were retained without additional peaks, suggesting that resveratrol was molecularly dispersed, with no chemical interaction with the lipid matrix, and these findings were similar to the previous study [36].

In the FTIR spectrum of sucrose, two prominent peaks at 3402 cm^{-1} and 3318 cm^{-1} indicated strong O-H stretching from chemically distinct alcohol groups [37]. Incorporating sucrose into lipid powder formulations preserved these characteristic peaks, showing no interaction between TRES and other components [38].

The FTIR spectrum of Tween 80 exhibited peaks at around 3600 (OH stretching), 2900 (CH_2 stretching), 1732.08 cm^{-1} (C=O stretching), and 1600 cm^{-1} (HOH bending) [39]. The SPC sample had peaks at 2922.82 cm^{-1} (CH_2 stretching) and 1736.27 cm^{-1} (C=O stretching), whereas Compritol 888 had a prominent peak at 2915 cm^{-1} that belonged to the C-H group. Another significant peak may be observed in the bands from 1586 to 1604 cm^{-1}, which corresponds to the C=C group, and from 1708 to 1738 cm^{-1}, this relates to the C=O group [40]. These peaks were also present in the corresponding formulations. Hence the formulations (F1–F15) were found to be stable and showed no signs of a chemical reaction that would have produced new functional groups.

3.2. PXRD analysis

The PXRD patterns of all formulations (F1-F15) along with sucrose and TRES are shown in Fig. 2. The PXRD pattern of pure TRES showed intense peaks at 2θ of 6.6, 16.4 and 19.1; and sucrose at 12.8, 18.9 and 25.2 confirmed their crystalline nature [35,41]. Moreover, in the PXRD patterns of all lipid-based formulations (F1-F15), no peaks for TRES were detected. This may suggest that whilst TRES is crystalline in its pure form, it becomes molecularly dispersed or amorphous when incorporated into the lipid matrix, consistent with previous studies [13,42]. However, high-intensity peaks of sucrose were observed in formulations (F1-F15), indicating the crystalline nature of the sucrose powder (Fig. 2). Furthermore, the peaks responsible for sucrose depicted an increase in intensity as the lipid-to-carrier ratio increased amongst formulations, where the lipid-to-sucrose carrier ratio elevated to 1:5, 1:10 and 1:15, respectively.

3.3. Surface morphology using SEM

The surface morphology of coarse sucrose, TRES, and the various lipid-based powder formulations (F1-F15) was analyzed using SEM (Fig. 3). SEM images revealed that sucrose particles (Fig. 3) were coarse, non-porous with sharp edges, and irregularly shaped but exhibited rough surfaces. Following the coating of the carrier with phospholipid (SPC), the surface roughness of sucrose diminished, particularly at a lipid-to-carrier ratio of 1:5 w/w (when compared to 1:15 w/w, lipid-to-carrier ratio), with increased lipid accumulation on the carrier's outer surface (Fig. 3). At the 1:05 w/w ratio, evidence of particle agglomeration was also noted; this may be attributed to the adhesive nature of the phospholipids (Fig. 3). These findings align with the results reported by Elhissi et al., [43] and Khan et al., [33]. A similar trend was observed across all other lipid-to-powder formulations that were prepared.

3.4. Characterization and analysis of particle size, PDI, zeta potential, and TRES entrapment

The particle size values measured for all the formulations (F1–F15) exhibited significant differences ($p < 0.05$), with values ranging from 101 to 2492 nm (Table 2). Upon analysis, it was observed that pro-niosome formulations (F4-F6) containing cholesterol exhibited larger

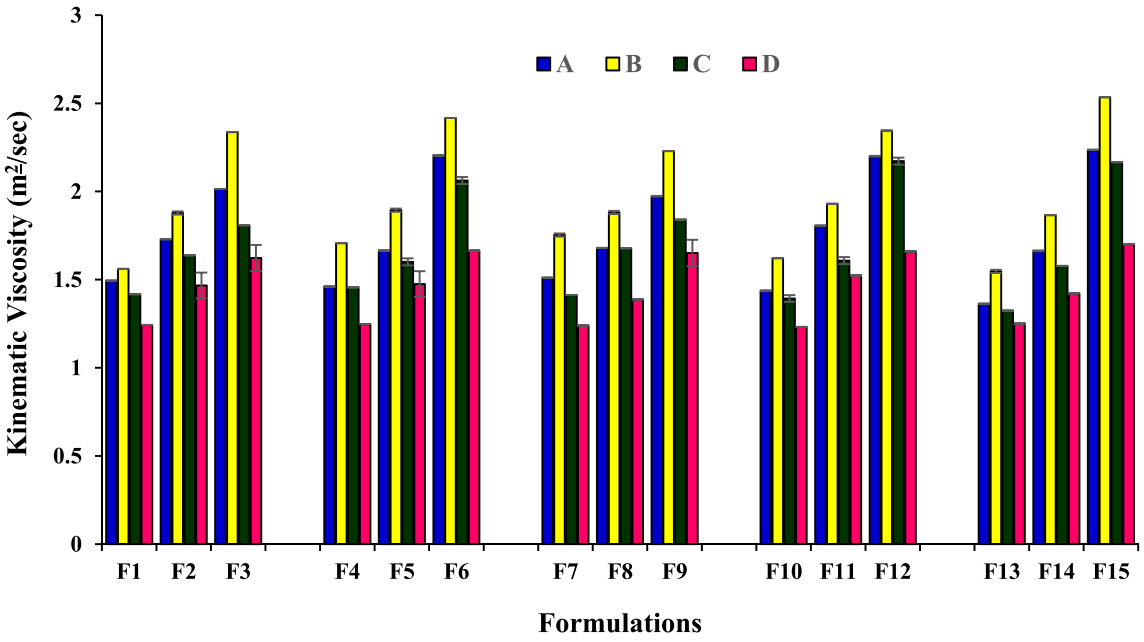

Fig. 4. Formulations (a) pro-micelles (F1-F3), (b) pro-niosomes (F4-F6), (c) pro-liposomes (F7-F9), (d) pro-transfersomes (F10-F12), and (e) pro-NLCs (F13-F15) were prepared in a dry powder form using three different ratios of lipid-to-sucrose carrier (1:05, 1:10, and 1:15 w/w). These formulations were then hydrated in water to form suspensions, and their kinematic viscosity was determined using four different types of Ubbelohde viscometers and referred to as A, B, C and D. Data are mean ± SD, n = 3.

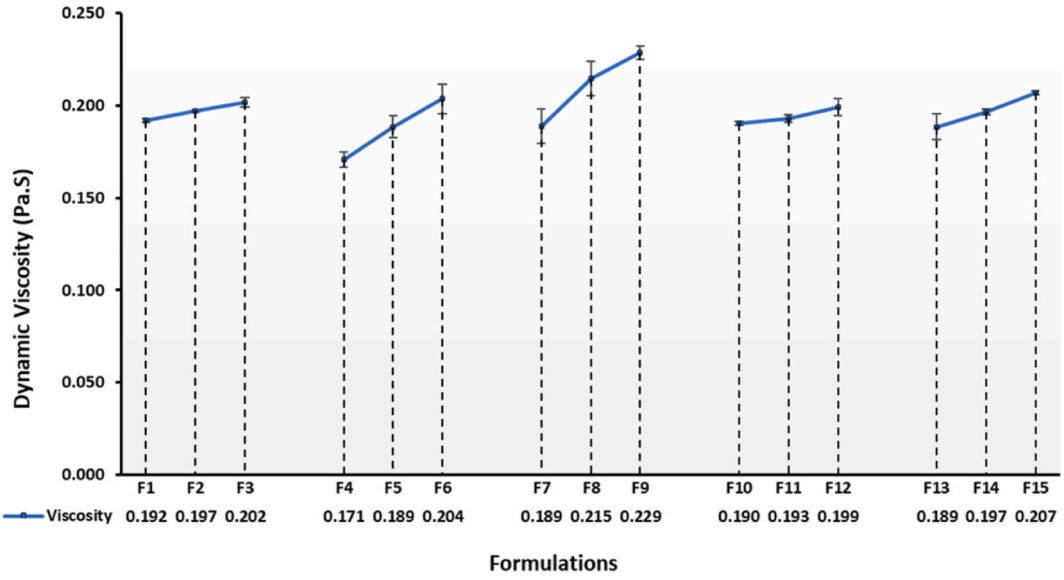

Fig. 5. The dynamic viscosity using a rheometer of the hydrated suspension formulations was measured for pro-micelles (F1-F3), pro-niosomes (F4-F6), pro-liposomes (F7-F9), pro-transfersomes (F10-F12), and pro-NLCs (F13-F15) in order to assess the correlation. Data are mean ± SD, n = 3.

particle sizes ($p < 0.05$) when compared to those without cholesterol (Table 1). The hydrophobicity of particle surfaces may rise with the addition of cholesterol, leading to particle aggregation and consequently, an increase in particle size. Moreover, the presence of cholesterol can also rigidify the niosomal matrix and integrate into the bilayer, which raises both the hydrodynamic diameter and particle size, as indicated by the PDI [44]. Low-angle X-ray diffraction studies showed that the surfactant bilayer became thicker by 3 Å when cholesterol was added. This increase in thickness likely reduces the area available per surfactant molecule within the membrane, contributing to larger vesicle size and PDI [45]. Whereas pro-transfersomes (F10-12) exhibited significantly smaller particle size ($p < 0.05$) than counterpart formulations. This may be attributed to the interaction of SPC and Tween 80 with the carbohydrate carrier, generating a hypertonic environment, which causes the lipid vesicles to shrink during hydration [46].

Notably, the incorporation of sucrose at different lipid-to-carrier ratios (1:5, 1:10, 1:15 w/w) resulted in a marked increase in particle size. This increase may be attributed to the concentration of the integrated carrier impacting the viscosity of the formulation. Higher carrier concentrations typically lead to increased viscosity, which can influence the rate of water transport into the bilayer. As the viscosity increases, this shows the movement of water into the lipid bilayer, but once water does enter, the increased pressure can facilitate further expansion of the

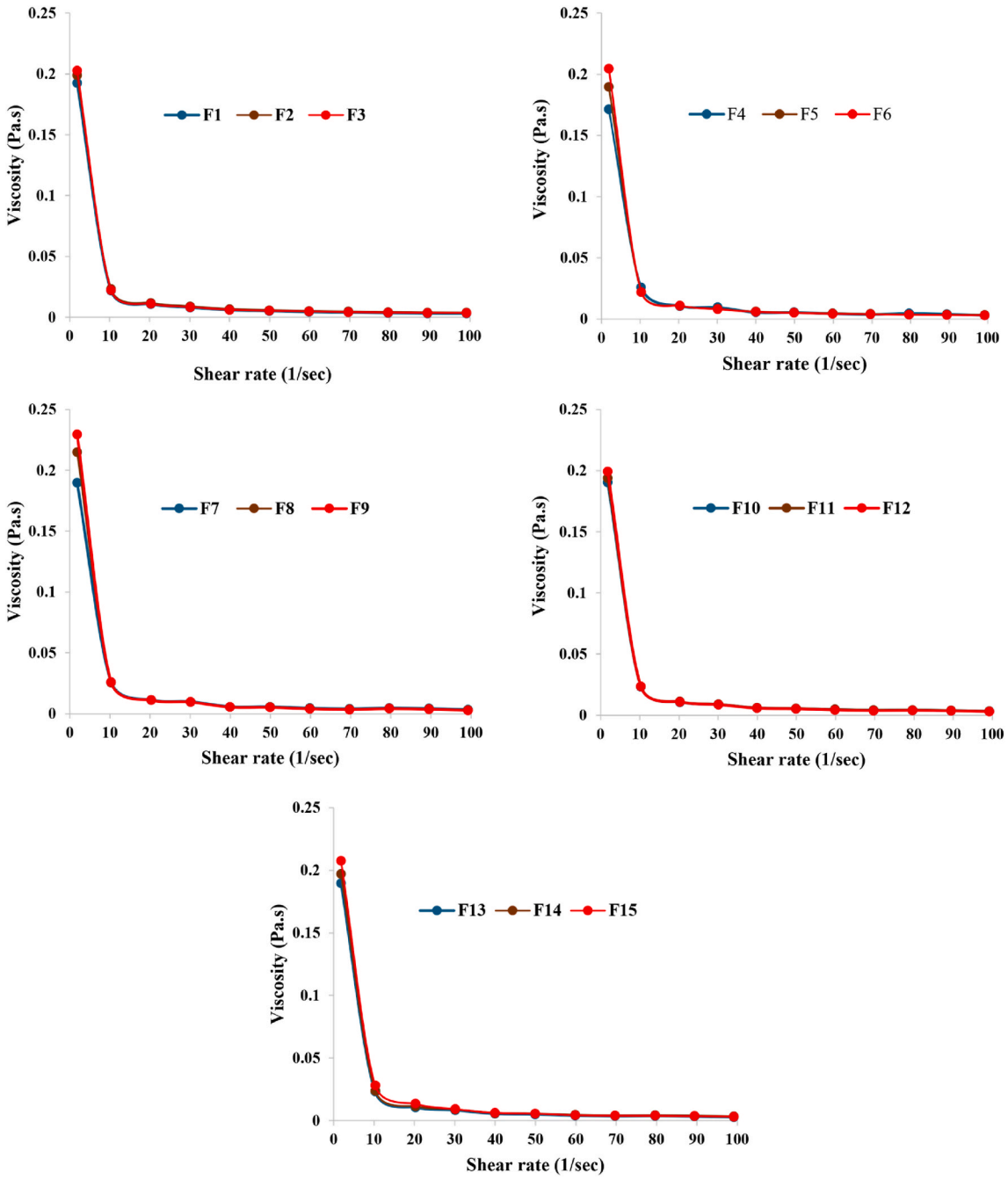

Fig. 6. Viscosity versus shear rate of all formulations was determined after hydration of pro-micelles (F1-F3), pro-niosomes (F4-F6), pro-liposomes (F7-F9), pro-transfersomes (F10-F12), and pro-NLCs (F13-F15) prepared using three different ratios of lipid-to-sucrose carrier (1:05, 1:10, and 1:15 w/w) at 25 °C. These formulations showed a shear-thinning behaviour. Data are mean ± SD, n = 3.

vesicle. Increased viscosity can enhance the stability of lipid nano-formulations by reducing particle mobility. This stabilization helps prevent aggregation and fusion of particles, maintaining a more uniform size distribution (PDI) [47,48]. Moreover, a PDI value of 0.3 or less demonstrates good uniformity between particles and is referred to as mono-dispersity [49]. The generated PDI values of all the formulations (i.e., F1–F15) exhibited PDI values ranging from 0.12 to 0.37 nm (Table 2).

The Zeta potential of all formulations (F1-F15) had a strong negative charge, with values ranging from −14 to −35 mV (Table 2). This may be attributed to the lipid particle's surface possessing OH- ions gained by absorbing hydroxyl ions from water [50]. Furthermore, the presence of endogenous surface-active compounds in oil, such as free fatty acids and glycerides, or polyphenol compounds like TRES, would cause the particle to become negatively charged [51].

Additionally, the EE of TRES in all the formulations (F1-F15) was measured using HPLC, showing efficiencies between 90 and 93% (Table 2). These outcomes align with previous research conducted by You et al., [52], which reported EE in lipid-based formulations reaching up to 87%. Similarly, Khan et al., [45] observed a high entrapment effectiveness of over 90% in pro-transfersome formulations. Greater EE may be related to the presence of long hydrocarbon chains of the phospholipid component (i.e., SPC), which may be able to entrap or accommodate higher TRES in the lipid bilayers [6]. The solubility of TRES in the lipid matrix may also offer high drug entrapment and reduce drug leakage. Thus, regardless of formulation type and viscosity, all

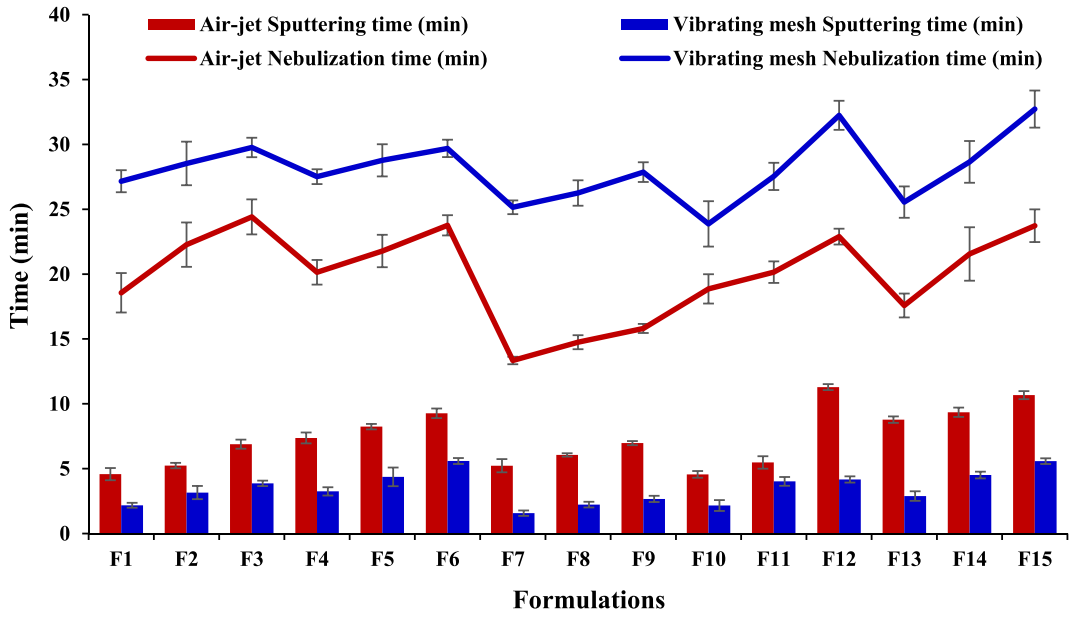

Fig. 7. Nebulization time (horizontal lines) and sputtering time (vertical bars) of the suspension formulation generated from TRES-loaded pro-micelles (F1-F3), pro-niosomes (F4-F6), pro-liposomes (F7-F9), pro-transfersomes (F10-F12), and pro-NLCs (F13-F15) were determined using two nebulizers (i.e., air-jet and vibrating mesh). All these formulations were prepared using three different ratios of lipid-to-sucrose carrier (1:05, 1:10, and 1:15 w/w). Data are mean ± SD, n = 3.

formulations (F1–F15) showed high EE (>90%) (Table 2).

3.5. Kinematic viscosity measurement using Ubbelohde viscometers

The viscosity of the formulations prepared from lipid-based formulations was measured *via* four different types of Ubbelohde viscometers (referred to as A, B, C, and D) to study the effect on nebulization performance. A direct correlation was observed between viscosity and the concentration of ingredients, specifically the lipid-to-sucrose ratio. This behaviour was observed after all the formulations (F1-F15) were hydrated with water, resulting in the formation of their respective vesicular systems. Upon hydration, they self-assembled into colloidal dispersions, and the viscosity measurements reflected the flow properties of the fully formed vesicles in aqueous media. Viscosity notably increased ($p < 0.05$) as sucrose concentrations rose (from a 1:5 to a 1:15 w/w lipid-to-carrier ratio) across all four types of Ubbelohde viscometers, irrespective of the formulation type (Fig. 4). The rise in sucrose concentration elevates osmotic pressure, causing water molecules to bind with sucrose and restrict movement, leading to higher viscosity [53]. Furthermore, sucrose forms more hydrogen bonds with water as concentration increases, strengthening the intermolecular interactions and ultimately decelerating the movement of molecules, resulting in increased viscosity [54].

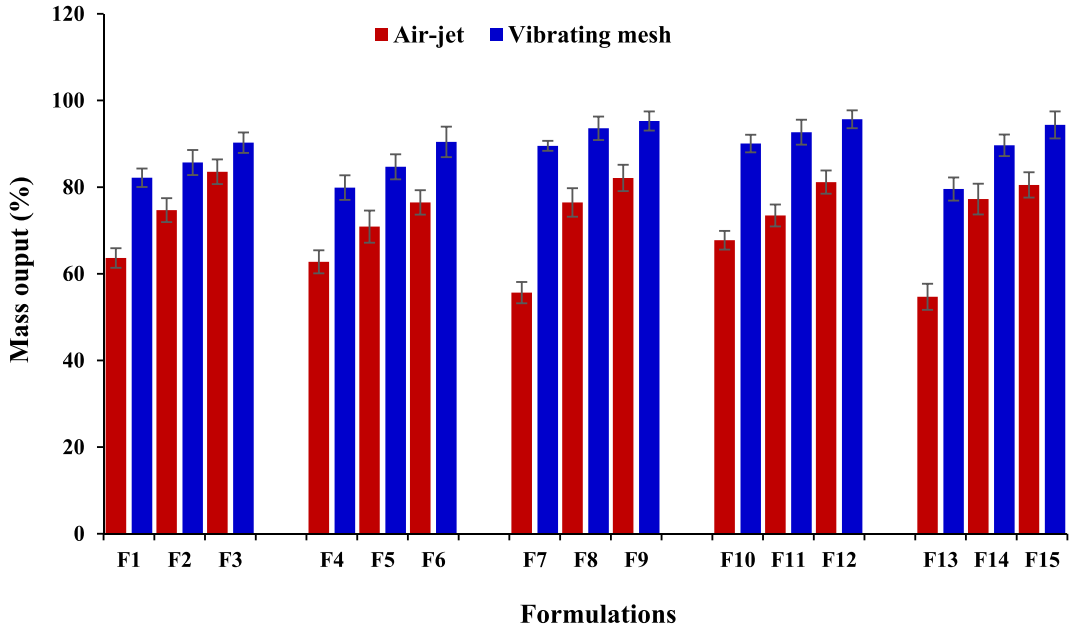

Fig. 8. Post-nebulization, the mass output of the suspension formulation generated from TRES-loaded pro-micelles (F1-F3), pro-niosomes (F4-F6), pro-liposomes (F7-F9), pro-transfersomes (F10-F12), and pro-NLCs (F13-F15) was determined using two nebulizers (i.e., air-jet and vibrating mesh). All these formulations were prepared using three different ratios of lipid-to-sucrose carrier (1:05, 1:10, and 1:15 w/w). Data are mean ± SD, n = 3.

Table 3
Nebulization performance of air-jet and vibrating mesh nebulizers using the suspension formulation generated from pro-micelles (F1-F3), pro-niosomes (F4-F6), pro-liposomes (F7-F9), pro-transfersomes (F10-F12), and pro-NLCs (F13-F15) formulations employing emitted dose (ED) and fine particle fraction (FPF) using TSI. Data are mean ± SD, n = 3.

Formulations	Vibrating mesh nebulizer		Air jet nebulizer	
	ED (%)	FPF (%)	ED (%)	FPF (%)
F1	93.10 ± 0.68	78.78 ± 0.48	80.55 ± 1.23	73.51 ± 1.10
F2	98.95 ± 0.91	81.90 ± 0.36	81.32 ± 1.78	77.61 ± 1.30
F3	94.73 ± 0.63	78.86 ± 1.87	81.72 ± 1.64	73.14 ± 0.39
F4	87.20 ± 0.68	72.74 ± 0.89	74.77 ± 0.75	69.68 ± 1.98
F5	91.73 ± 1.78	80.59 ± 1.23	87.91 ± 0.85	69.38 ± 1.74
F6	81.16 ± 0.84	73.90 ± 0.35	77.23 ± 1.48	70.49 ± 0.54
F7	91.53 ± 0.98	78.72 ± 0.75	88.91 ± 2.48	73.21 ± 0.86
F8	88.06 ± 1.89	69.11 ± 0.86	84.32 ± 1.19	62.04 ± 0.78
F9	87.06 ± 1.34	71.97 ± 0.70	83.53 ± 1.75	67.30 ± 1.96
F10	95.78 ± 0.83	80.43 ± 1.65	83.14 ± 1.75	73.29 ± 1.78
F11	96.10 ± 0.65	74.06 ± 1.45	91.94 ± 1.89	69.62 ± 0.89
F12	86.83 ± 1.20	71.19 ± 1.09	81.60 ± 1.03	64.89 ± 0.12
F13	72.30 ± 0.24	60.02 ± 1.36	60.58 ± 0.54	52.91 ± 1.56
F14	89.25 ± 0.12	72.49 ± 0.64	84.61 ± 0.87	67.15 ± 1.23
F15	88.08 ± 0.24	78.70 ± 0.64	77.47 ± 0.99	70.20 ± 1.10

3.6. Dynamic viscosity measurements using rheometer

The dynamic viscosity of all the lipid-based formulations (F1-F15) was measured using a rheometer (i.e., viscosity as a function of shear rate) (Fig. 5). The results obtained demonstrated a similar trend to that determined using four different types of Ubbelohde viscometers, irrespective of formulation type. However, it is important to know that a significant difference ($p < 0.05$) was identified within the same type of lipid-based formulations, particularly between lower and higher concentration where an increasing sucrose carrier concentration caused an elevation in viscosity. The viscosity values ranged between 0.17 and 0.23 Pa s (Fig. 5).

The relationship between viscosity and shear rate demonstrated non-Newtonian flow behaviour, characterized by shear-thinning or pseudoplastic properties, where viscosity decreased as shear rate increased (Fig. 6). This phenomenon is due to the rearrangement of the fluid's microstructure along the plane of applied shear. As shear stress increases, the internal structure of the system, such as vesicle alignment, deformation or disruption, results in reduced resistance to flow, hence lowering the viscosity. This shear-induced thinning is particularly dependent on the lipid-to-sucrose ratio in different formulation systems [6].

3.7. Analysis of nebulization time, sputtering time and mass output

Nebulization time is the time required for aerosolization, where the formation of the aerosol becomes erratic (Fig. 7). Nebulization performance, specifically droplet size and nebulization time, was significantly affected by the formulation's viscosity, surface tension, and the types of ions present in the suspension. These factors interact with the nebulizer's design and operational method, influencing overall efficiency [55]. Vesicles hydrated from all the lipid-based formulations with increasing lipid-to-sucrose carrier ratios (1:05, 1:10, and 1:15 w/w) exhibited a significant increase ($p < 0.05$) in terms of nebulization time (within each type of lipid-based formulation) while using both an air jet and vibrating mesh nebulizers. The difference in nebulization performance is likely due to variations in dispersion viscosity from using different lipid-to-sucrose carrier concentrations. Formulations with lower viscosity may allow faster release of aerosol from the nebulizers [55]. In contrast, higher lipid concentrations result in more viscous formulations, leading to longer nebulization times. Viscosity measurements also confirmed that increasing the sucrose carrier content raised the viscosity of the lipid-based formulations (Figs. 4 and 5). The higher viscosity may affect nebulization time, as explained by Finlay et al., [56], who proposed that the higher the viscosity, the greater the adherence of aerosol droplets to the inner walls of the nebulizer, followed by the reduced defection of these droplets into the nebulizer reservoir, greatly extending the nebulization time [56,57]. Because of increasing lipid buildup within the nebulizer towards the end of nebulization, this may cause a marginal degree aggregation and/or fusion, resulting in extended nebulization. These findings indicate that using a lower ratio of lipid-to-carrier (1:05) was more appropriate if the aim was to accomplish nebulization quickly.

Furthermore, nebulization time is also affected by nebulizer type and design, with vibrating mesh devices being more formulation-sensitive than air-jet nebulizers. Upon analysis, vibrating mesh nebulizers demonstrated significantly longer ($p < 0.05$) nebulization time when compared to air-jet nebulizers. The longer nebulization time may be attributed to the lower energy of atomization during nebulization. Furthermore, it may produce nanoparticle aggregation/fusion, which may result in mesh obstruction and, as a result, extended nebulization time.

Sputtering time also varied significantly ($p < 0.05$) amongst air jet and vibrating mesh nebulizers. Upon comparison, a significant difference ($p < 0.05$) in formulation sputtering times was observed between the lower and higher lipid-to-carrier ratios when employing both an air-jet and vibrating mesh nebulizers. Increasing carrier concentration resulted in increasing sputtering time (Fig. 7). Trends observed in sputtering time mirrored with trends in nebulization time, and were in agreement with findings outlined by Khan et al., [45]. When compared to the air-jet nebulizer, the design of the vibrating mesh nebulizer maintained a lower proportion of the formulation post-nebulization (the majority/proportion of the formulation was aerosolized and hence took longer nebulization time) and thus displayed a significantly shorter ($p < 0.05$) sputtering duration than air-jet nebulizer.

It is noteworthy that sucrose plays a key role in stabilizing the dry formulation and facilitating nanosuspension formation upon hydration. In dry powder formulations, sucrose acts as a solid stabilizing matrix that decreases aggregation of lipid components during solvent evaporation (i.e., ethanol evaporation *via* rotary evaporator) and storage. It has also been widely reported that sugars as carriers stabilize lipid assemblies during dehydration through hydrogen bonding with polar lipid head groups [58,59]. Upon hydration, sucrose swiftly dissolves, facilitating effective dispersion and self-assembly of lipid components into nanoscale particles/vesicles prior to nebulization, which is important for maintaining stable suspensions and consistent aerosol generation. Preservation and maintenance of nanoscale particle size after reconstitution/hydration is important for consistent nebulization behaviour, since instability or aggregation can adversely affect the generation of aerosol, distribution of droplet size, and hence efficiency of pulmonary delivery. Moreover, at a lower lipid-to-sucrose ratio, the concentration of sucrose may be insufficient to fully protect the lipid interface, whereas the excess sugar matrix may alter redispersion efficiency, increase viscosity, and potentially impact drug release behaviour.

It is not possible to reach 100% mass output regardless of nebulizer type, nebulization to dryness, or total nebulization time (combined time length of nebulization time and sputtering time). The air-jet nebulizer demonstrated much lower mass output ($p < 0.05$) than the vibrating mesh nebulizer (Fig. 8). This difference may be attributed to the nebulizer's design. The air-jet nebulizer is associated with a tendency to retain a high residual volume in its reservoir. In contrast, the vibrating mesh nebulizer has a slanted reservoir, which promotes better flow of the formulation towards the perforated plate, enhancing aerosol production. This design minimizes formulation retention and prevents the deflection of the formulation back into the reservoir (lower deposition of formulation on the internal walls), ensuring more efficient aerosolization [60]. These outcomes demonstrate that nebulizer design and formulation physicochemical properties impact upon mass output.

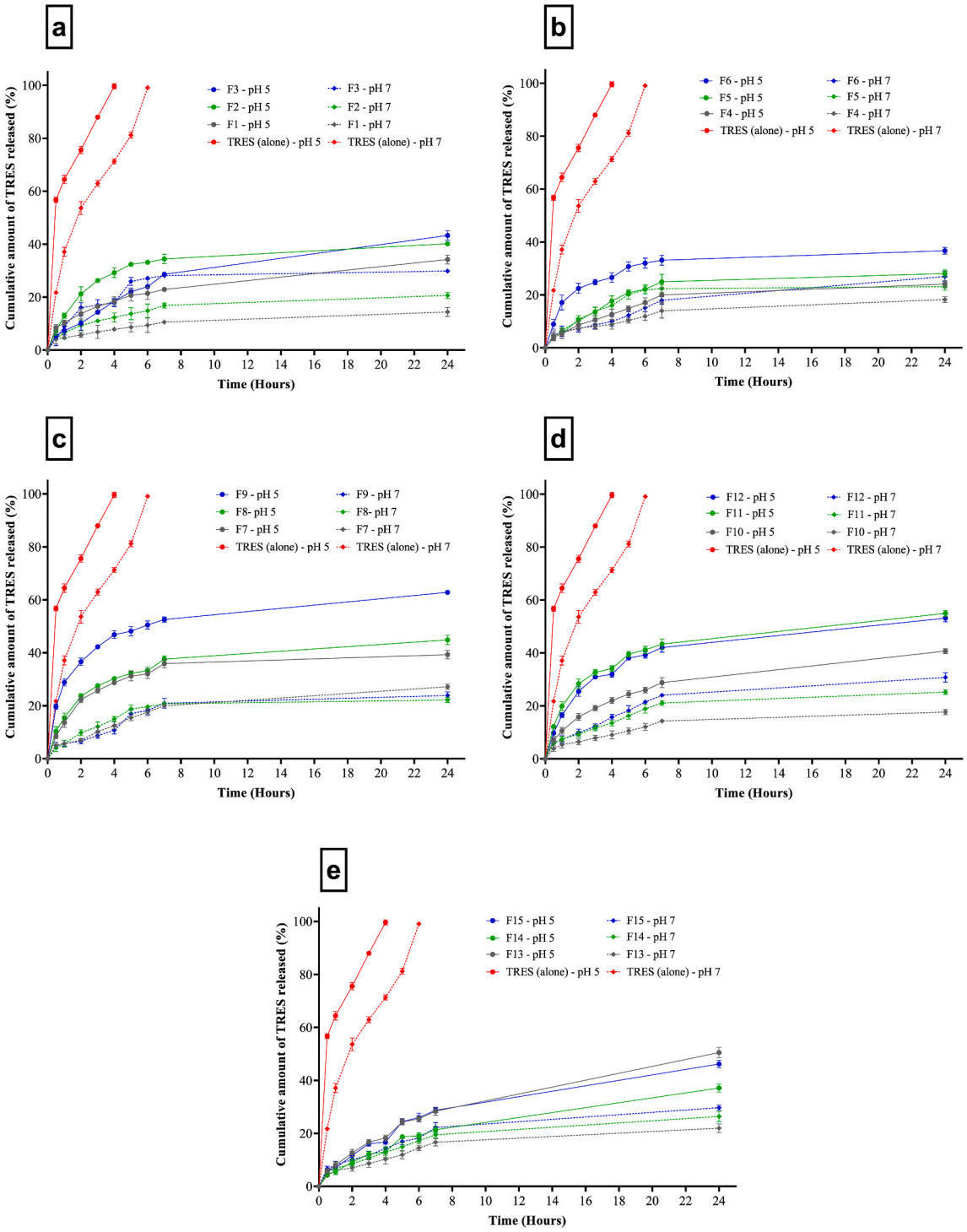

Fig. 9. *In-vitro* release of TRES alone (used as a control), and TRES release from the suspension formulation generated from: (a) pro-micelles (F1-F3), (b) pro-niosomes (F4-F6), (c) pro-liposomes (F7-F9), (d) pro-transfersomes (F10-F12), and (e) pro-NLCs (F13-F15) formulations. All these formulations were prepared using three different ratios of lipid-to-sucrose carrier (1:05, 1:10, and 1:15 w/w). Data are mean ± SD, n = 3.

3.8. TRES deposition in TSI, post nebulization

TRES deposition in both the upper and lower stages (also known as emitted dose (ED)) of TSI as well as formulations remaining in the nebulizer reservoir containing TRES was determined *via* HPLC post-nebulization. Both ED and FPF demonstrated significantly higher ($p < 0.05$) deposition of TRES when a vibrating mesh nebulizer was employed as compared to an air-jet nebulizer (Table 3). This trend may be related to the design and mechanisms of the nebulizers. The higher ED and FPF may be related to the lower residual/dead volume remaining after nebulization when a vibrating mesh was employed. Similar findings were also observed for higher FPF when a vibrating mesh nebulizer was employed using lipid-based formulations [6,61]. Whereas, when using an air-jet nebulizer, the formulation may adhere to the internal walls of the nebulizer, leading to the presence of a higher residual volume (also demonstrated by a shorter nebulization time). The higher the residual volume, the lower the ED, and hence the lower the FPF.

3.9. In-vitro drug release studies on prepared formulations

The cumulative concentration of TRES released from all formulations (F1-F15), along with TRES alone as a control, was studied in two different pH environments: acetate buffer (pH-5) and DW (pH-7) (Fig. 9). The TRES release pattern of all the lipid-based formulations depicted the zero-order controlled drug release (decreasing positive slopes confirm that the drug was released *via* pure diffusion) due to the release of TRES at a constant rate from all the lipid-based formulations over time [62]. This matches the ultimate goal of using lipid formulations to deliver the drugs in a controlled manner, as it increases the therapeutic effect of the drug.

In 4 h, TRES alone achieved 100% release at pH 5 and 80% at pH 7 (Fig. 9). Pro-niosomes (F4-F6) depicted the lowest TRES release regardless of the release media. This may be attributed to the presence of cholesterol in pro-niosome formulations, which may enhance the packing of lipid chains and bilayer formation, thereby reducing membrane fluidity and rigidity, which in turn hinders the movement of the drug from within the vesicles to the outside environment. Moreover, the release profile of TRES at pH 5 was significantly higher ($p < 0.05$) than at pH 7 (Fig. 9). This difference may be attributed to the TRES hydrophobic characteristics, which reduced its affinity for water, affecting release rates in a pH 7 environment. It is well established that lung tumours generate and export excess lactic acid due to upregulated glycolytic metabolism, resulting in strongly acidic extracellular pH in the tumour microenvironment that is typically $\leq$ pH 7. It was reported that TRES remains stable in acidic environments, while its degradation rate increases exponentially in alkaline pH (6.8-9.0) [63]. Therefore, TRES had higher stability at lower pH conditions. Additionally, a general trend of higher drug release was observed with formulations with higher sucrose concentration and viscosity.

4. Conclusions

The study aimed to investigate how the significance of the sucrose concentrations in a range of lipid-based formulations (F1-F15), and how this affects the resultant physicochemical properties and nebulization performance in pulmonary drug delivery. This impact was assessed *via* a TSI in combination with air-jet and vibrating mesh nebulizers. Upon increasing the sucrose ratio, there was an increase in particle size and higher PDI values. Similarly, upon using Ubbelohde viscometers, increasing the sucrose concentration (from a 1:5 to a 1:15 w/w ratio) resulted in greater flow resistance and higher viscosity. In contrast, measurements with a rotational viscometer exhibited non-Newtonian behaviour, as viscosity decreased with increasing shear rate. The nebulization performance indicated that formulations with lower viscosity (when prepared in a ratio of 1:5 w/w) resulted in shorter nebulization time and sputtering time. Moreover, based on drug deposition in the TSI using two nebulizers, the vibrating mesh nebulizer demonstrated superior performance compared to the air-jet nebulizer (irrespective of sucrose concentrations). Hence, vibrating mesh nebulizer and formulations with lower sucrose concentrations were identified as the best combination for pulmonary drug delivery.

CRediT authorship contribution statement

Anila Mathew Thevarkattil: Methodology, Writing – original draft. **Kajanthan Balasundaram:** Data curation, Formal analysis, Methodology. **Nozad Hussein:** Data curation, Validation. **Huner Omer:** Software, Visualization. **Sakib Yousaf:** Investigation, Writing – review & editing. **Chahinez Houacine:** Resources, Validation. **Adeeb Shehzad:** Software, Visualization. **Ruba Bnyan:** Formal analysis, Resources. **Abdelbary Elhissi:** Investigation, Validation. **Iftikhar Khan:** Conceptualization, Project administration, Supervision, Writing – review & editing.

Declaration of competing interest

The authors declare that they have no known competing financial interests or personal relationships that could have appeared to influence the work reported in this paper.

Appendix A. Supplementary data

Supplementary data to this article can be found online at https://doi.org/10.1016/j.jddst.2026.108671.

Data availability

Data will be made available on request.

References

[1] B.C. Bade, C.S.D. Cruz, Lung cancer 2020: epidemiology, etiology, and prevention, Clin. Chest Med. 41 (2020) 1–24.
[2] M. Apostolou, A.A. Fatokun, S. Assi, I. Khan, Targeted lipid-based drug delivery systems for lung cancer therapy, Appl. Sci. 14 (2024) 6759.
[3] T. Tatsumura, K. Yamamoto, A. Murakami, M. Tsuda, S. Sugiyama, New chemotherapeutic method for the treatment of tracheal and bronchial cancers–nebulization chemotherapy, Gan no rinsho. Japan journal of cancer clinics 29 (1983) 765–770.
[4] W.H. Roa, S. Azarmi, M.K. Al-Hallak, W.H. Finlay, A.M. Magliocco, R. Löbenberg, Inhalable nanoparticles, a non-invasive approach to treat lung cancer in a mouse model, J. Contr. Release 150 (2011) 49–55.
[5] S. Subramanian, I. Khan, O. Korale, M.A. Alhnan, W. Ahmed, M. Najlah, K. M. Taylor, A. Elhissi, A simple approach to predict the stability of phospholipid vesicles to nebulization without performing aerosolization studies, Int. J. Pharm. 502 (2016) 18–27.
[6] A. Mathew Thevarkattil, S. Yousaf, C. Houacine, W. Khan, R. Bnyan, A. Elhissi, I. Khan, Anticancer drug delivery: investigating the impacts of viscosity on lipid-based formulations for pulmonary targeting, Int. J. Pharm. 664 (2024) 124591.
[7] C. Houacine, I. Khan, S.S. Yousaf, Potential cardio-protective agents: a resveratrol review (2000-2019), Curr. Pharm. Des. 27 (2021) 2943–2955.
[8] A.R. Neves, M. Lúcio, J.L.C. Lima, S. Reis, Resveratrol in medicinal chemistry: a critical review of its, Food Chem. 47 (1999) 4456–4461.
[9] M. Athar, J.H. Back, X. Tang, K.H. Kim, L. Kopelovich, D.R. Bickers, A.L. Kim, Resveratrol: a review of preclinical studies for human cancer prevention, Toxicol. Appl. Pharmacol. 224 (2007) 274–283.
[10] B. Li, O.Q.B. Allela, W.H. Alkhazali, N. Vadia, S. Renuka Jyothi, R. Panigrahi, A. S. Chauhan, S. Singh, M. Akhrorova, H.N. Sameer, et al., Resveratrol in oral cancer: a systematic review of preclinical studies on its anticancer mechanisms and therapeutic potential, Med. Oncol. 42 (2025) 329.
[11] C.A. Hunt, S. Tsang, A-tocopherol retards autoxidation and prolongs the shelf-life of liposomes, Int. J. Pharm. 8 (1981) 101–110.
[12] P. Bhardwaj, P. Tripathi, R. Gupta, S. Pandey Niosomes, A review on niosomal research in the last decade, J. Drug Deliv. Sci. Technol. 56 (2020) 101581.
[13] I. Khan, A. Al-Hasani, M.H. Khan, A.N. Khan, F.E. Alam, S.K. Sadozai, A. Elhissi, J. Khan, S. Yousaf, Impact of dispersion media and carrier type on spray-dried proliposome powder formulations loaded with beclomethasone dipropionate for their pulmonary drug delivery via a next generation impactor, PLoS One 18 (2023) e0281860.
[14] N.I. Payne, C.V. Ambrose, P. Timmins, M.D. Ward, F. Ridgway Proliposomes, A novel solution to an old problem, J. Pharmaceut. Sci. 75 (1986) 325–329.
[15] I. Khan, K. Edes, I. Alsaadi, M.Q. Al-Khaial, R. Bnyan, S.A. Khan, S.K. Sadozai, W. Khan, S. Yousaf, Investigation of spray drying parameters to formulate novel spray-dried proliposome powder formulations followed by their aerosolization performance, Pharmaceutics 16 (2024).
[16] J.R. Madan, N.P. Ghuge, K. Dua, Formulation and evaluation of proniosomes containing lornoxicam, Drug Deliv. Transl. Res. 6 (2016) 511–518.
[17] T.C. Carvalho, J.T. McConville, The function and performance of aqueous aerosol devices for inhalation therapy, J. Pharm. Pharmacol. 68 (2016) 556–578.
[18] A. Elhissi, D. Elkhalifa, I. Khan, W. Ahmed, Introduction: pulmonary drug delivery and inhalation devices, in: A. Elhissi, D. Elkhalifa, I. Khan, W. Ahmed (Eds.), Proliposomes: a Manufacturing Technology of Liposomes for Pulmonary Drug Delivery, Springer Nature Switzerland, Cham, 2025, pp. 1–34.
[19] C. Darquenne, G.K. Prisk, Aerosol deposition in the human respiratory tract breathing air and 80: 20 heliox, J. Aerosol Med. 17 (2004) 278–285.
[20] E.-Z. Papavasileiou, D.M. Rekkas, P.P. Dallas, S. Pispas, N. Pippa, Unlocking the potential of micelles: doe and qbd strategies for formulation development and optimization, J. Drug Deliv. Sci. Technol. 115 (2026) 107795.
[21] N. Eczacioglu, M.H. Asim, S. Haddadzadegan, A. Bernkop-Schnürch, Liquid crystalline inverted lipid phases and reverse micelles in drug delivery: from molecular design to therapeutic potential, Adv. Funct. Mater. (2025) e22873 n/a.
[22] R. Vallala, B. Daravath, Niosomes in drug delivery: a comprehensive review and therapeutic perspectives, Nanotechnology 9 (2026) 100440.

[23] J. Bag, S. Mukhopadhyay, G. Nandi, H.M. Tun, Next-generation composite vesicular systems: an in-depth review of proniosomes in advanced drug delivery, Drug Deliv. 33 (2026) 2614585.
[24] K. Safari, I. Pitterou, M. Miliaronikolaki, N. Paraskevopoulos, A. Tzani, A. Detsi, Nanostructured lipid carriers and natural deep eutectic solvents: a highly advantageous combination for the encapsulation of curcumin, J. Chem. Technol. Biotechnol. (2025) n/a.
[25] U.A. Havelikar, S.B. Magar, A.K. Teharke, N.B. Chaudhari, Recent approaches of proliposome-based dry powder inhalation for pulmonary delivery, J. Drug Deliv. Sci. Technol. 117 (2026) 108053.
[26] N. Čutović, P. Batinić, T. Marković, J. Petrović, M. Obradović, B. Bugarski, A. A. Jovanović, Comparative study of natamycin encapsulation in liposomes: Thin-film vs. Proliposome methods for enhanced stability, controlled release, and efficacy against milk spoilage and pathogenic microorganisms 14 (2025) 3064.
[27] H. Manjushree, D. Nayak, P. Halagali, M. Rathnanand, R. Tawale, K. Ananthmurthy, J.M. Aranjani, V.K. Tippavajhala, Menthol-based novel ultra-deformable vesicle: formulation, optimization and evaluation of an antifungal drug, AAPS PharmSciTech 26 (2025) 23.
[28] L. Casula, M. Vitek, A. Zvonar Pobirk, M. Gosenca Matjaž, D. Valenti, A. Dupont, C. Caddeo, Design and optimisation of phospholipid vesicles for topical betamethasone dipropionate, Eur. J. Pharmaceut. Sci. 216 (2026) 107363.
[29] N.T. Ozaksun, T. Tayyar, A. Ozdemir, M. Ark, T. Incecayir, Development and optimization of soluplus®/pluronic-based polymeric micelles for bicalutamide delivery: characterization, lyophilization, stability, and cellular studies, Eur. J. Pharmaceut. Sci. 217 (2026) 107395.
[30] N.F. Younes, S. Sayed, M. Hassan, S. Ahmed, Engineered lecithin-based proniosomes for enhanced trans-tympanic permeation: in vitro, microbiological, ex vivo and in vivo evaluation, J. Drug Deliv. Sci. Technol. 96 (2024) 105728.
[31] A. Ruppl, D. Kiesewetter, M. Köll-Weber, T. Lemazurier, R. Süss, A. Allmendinger, Formulation screening of lyophilized mrna-lipid nanoparticles, Int. J. Pharm. 671 (2025) 125272.
[32] D. Guimarães, J. Noro, C. Silva, A. Cavaco-Paulo, E. Nogueira, Protective effect of saccharides on freeze-dried liposomes encapsulating drugs, Front. Bioeng. Biotechnol. 7 (2019) 424.
[33] I. Khan, S. Yousaf, S. Subramanian, O. Korale, M.A. Alhnan, W. Ahmed, K.M. G. Taylor, A. Elhissi, Proliposome powders prepared using a slurry method for the generation of beclometasone dipropionate liposomes, Int. J. Pharm. 496 (2015) 342–350.
[34] I. Khan, M. Sabu, N. Hussein, H. Omer, C. Houacine, W. Khan, A. Elhissi, S. Yousaf, Trans-resveratrol-loaded nanostructured lipid carrier formulations for pulmonary drug delivery using medical nebulizers, J. Pharmaceut. Sci. 114 (2025) 103713.
[35] R. Sun, G. Zhao, S. Ni, Q. Xia, Lipid based nanocarriers with different lipid compositions for topical delivery of resveratrol: comparative analysis of characteristics and performance, J. Drug Deliv. Sci. Technol. 24 (2014) 591–600.
[36] J. Sun, Y. Zhou, Y. Su, S. Li, J. Dong, Q. He, Y. Cao, T. Lu, L. Qin, Resveratrol-loaded solid lipid nanoparticle supplementation ameliorates physical fatigue by improving mitochondrial quality control, Crystals 9 (2019) 559.
[37] B.C. Smith, An Ir Spectral Interpretation Potpourri: Carbohydrates and Alkynes, 2017.
[38] B.C. Smith, Infrared Spectral Interpretation: a Systematic Approach, CRC press, 2018.
[39] K. Pramod, C.V. Suneesh, S. Shanavas, S.H. Ansari, J. Ali, Unveiling the compatibility of eugenol with formulation excipients by systematic drug-excipient compatibility studies, J. Anal. Sci. Technol. 6 (2015) 34.
[40] A. Tatke, N. Dudhipala, K.Y. Janga, S.P. Balguri, B. Avula, M.M. Jablonski, S. Majumdar, In situ gel of triamcinolone acetonide-loaded solid lipid nanoparticles for improved topical ocular delivery: tear kinetics and ocular disposition studies, Nanomaterials 9 (2018) 33.
[41] A.L. Voelker, C. Felten, L.S. Taylor, L.J. Mauer, Effects of polyphenols on crystallization of amorphous sucrose lyophiles, Food Chem. 338 (2021) 128061.
[42] A. Ebrahimi, M. Saffari, T. Langrish, Developing a new production process for high-porosity lactose particles with high degrees of crystallinity, Powder Technol. 272 (2015) 45–53.
[43] A.M.A. Elhissi, W. Ahmed, D. McCarthy, K.M.G. Taylor, A study of size, microscopic morphology, and dispersion mechanism of structures generated on hydration of proliposomes, J. Dispersion Sci. Technol. 33 (2012) 1121–1126.
[44] P. Shah, B. Goodyear, A. Haq, V. Puri, B. Michniak-Kohn, Evaluations of quality by design (qbd) elements impact for developing niosomes as a promising topical drug delivery platform, Pharmaceutics 12 (2020) 246.
[45] I. Khan, R. Needham, S. Yousaf, C. Houacine, Y. Islam, R. Bnyan, S.K. Sadozai, M. A. Elrayess, A. Elhissi, Impact of phospholipids, surfactants and cholesterol selection on the performance of transfersomes vesicles using medical nebulizers for pulmonary drug delivery, J. Drug Deliv. Sci. Technol. 66 (2021) 102822.
[46] J. Lehtonen, P. Kinnunen, Changes in the lipid dynamics of liposomal membranes induced by poly (ethylene glycol): free volume alterations revealed by inter-and intramolecular excimer-forming phospholipid analogs, Biophys. J. 66 (1994) 1981–1990.
[47] M. Laura Immordino, F. Dosio, L. Cattel, Stealth liposomes: review of the basic science, rationale, and clinical applications, existing and potential, Int. J. Nanomed. 1 (2006) 297–315.
[48] N.R. Hussein, Spray-dried liposomes: a study of the effect of carbohydrate carrier and concentrations on liposome size and drug entrapment, Zanco Journal of Medical Sciences (Zanco J Med Sci) 23 (2019) 345–353.
[49] M. Danaei, M. Dehghankhold, S. Ataei, F. Hasanzadeh Davarani, R. Javanmard, A. Dokhani, S. Khorasani, y.M. Mozafari, Impact of particle size and polydispersity index on the clinical applications of lipidic nanocarrier systems, Pharmaceutics 10 (2018) 57.
[50] P. Witayaudom, U. Klinkesorn, Effect of surfactant concentration and solidification temperature on the characteristics and stability of nanostructured lipid carrier (nlc) prepared from rambutan (Nephelium lappaceum l.) kernel fat, J. Colloid Interface Sci. 505 (2017) 1082–1092.
[51] D. Pandita, S. Kumar, N. Poonia, V. Lather, Solid lipid nanoparticles enhance oral bioavailability of resveratrol, a natural polyphenol, Food Res. Int. 62 (2014) 1165–1174.
[52] Y.-y. You, X.-b. Suo, J.-j. Yue, X. Xu, H. Zhang, Determination of entrapment efficiency of liposomal paclitaxel by rp-hplc, Chinese Journal of Pharmaceutical Analysis 37 (2017) 535–539.
[53] T. Söderlund, J.-M.I. Alakoskela, A.L. Pakkanen, P.K. Kinnunen, Comparison of the effects of surface tension and osmotic pressure on the interfacial hydration of a fluid phospholipid bilayer, Biophys. J. 85 (2003) 2333–2341.
[54] O. Tas, U. Ertugrul, L. Grunin, M.H. Oztop, Investigation of the hydration behavior of different sugars by time domain-nmr, Foods 11 (2022) 1148.
[55] T. Ghazanfari, A.M. Elhissi, Z. Ding, K.M. Taylor, The influence of fluid physicochemical properties on vibrating-mesh nebulization, Int. J. Pharm. 339 (2007) 103–111.
[56] W.H. Finlay, C.F. Lange, M. King, D.P. Speert, Lung delivery of aerosolized dextran, Am. J. Respir. Crit. Care Med. 161 (2000) 91–97.
[57] I. Khan, S. Sunita, N.R. Hussein, H.K. Omer, A. Elhissi, C. Houacine, W. Khan, S. Yousaf, H.A. Rathore, Development and characterization of novel combinations and compositions of nanostructured lipid carrier formulations loaded with trans-resveratrol for pulmonary drug delivery, Pharmaceutics 16 (2024) 1589.
[58] J.H. Crowe, J.F. Carpenter, L.M. Crowe, The role of vitrification in anhydrobiosis, Annu. Rev. Physiol. 60 (1998) 73–103.
[59] W. Abdelwahed, G. Degobert, S. Stainmesse, H. Fessi, Freeze-drying of nanoparticles: formulation, process and storage considerations, Adv. Drug Deliv. Rev. 58 (2006) 1688–1713.
[60] I. Khan, S. Hussein, C. Houacine, S.K. Sadozai, Y. Islam, R. Bnyan, A. Elhissi, S. Yousaf, Fabrication, characterization and optimization of nanostructured lipid carrier formulations using beclomethasone dipropionate for pulmonary drug delivery via medical nebulizers, Int. J. Pharm. 598 (2021) 120376.
[61] M.E. Abdelrahim, P. Plant, H. Chrystyn, In-vitro characterisation of the nebulised dose during non-invasive ventilation, J. Pharm. Pharmacol. 62 (2010) 966–972.
[62] S. Adepu, S. Ramakrishna, Controlled drug delivery systems: current status and future directions, Molecules 26 (2021) 5905.
[63] B.C. Trela, A.L. Waterhouse, Resveratrol: isomeric molar absorptivities and stability, J. Agric. Food Chem. 44 (1996) 1253–1257.